Computer simulation of the skin reflectance spectra

I.V. Meglinski [a],*, S.J. Matcher [b]

[a] School of Engineering, Cranfield University, Cranfield MK43 0AL, UK
[b] School of Physics, University of Exeter, Exeter EX4 4QL, UK

Abstract

The reflectance spectra of the human skin in visible and near-infrared (NIR) spectral region have been calculated using the Monte Carlo technique, and the specular and internal reflection on the medium surface is taken into account. Skin is represented as a complex inhomogeneous multi-layered highly scattering and absorbing medium. The model takes into account variations in spatial distribution of blood, index of blood oxygen saturation, volume fraction of water and chromophores content. The simulation of the skin tissues optical properties and skin reflectance spectra are discussed. Comparison of the results of simulation and in vivo experimental results are given.

Keywords: Skin reflectance spectra; Monte Carlo; Multi-layered medium; Skin tissues optical properties

1. Introduction

The in vivo spectral reflectance measurements of human skin can serve as a valuable supplement to standard non-invasive techniques for diagnosing various skin diseases, such as venous ulcers, skin necrosis, interstitial oedema, etc. However, quantified analysis of the reflectance spectra is complicated by the fact that skin has a complex multi-layered non-homogeneous structure [1,2] with a spatially varying absorption coefficient, mainly determined by melanin pigmentation, oxygen saturation of cutaneous blood, index of erythema, bilirubin, β-carotine and other chromophores [3].

In most of clinical applications given the measured reflectance spectra, we need to extract the concentrations of various chromophores of interest, in particular oxy- and deoxy-hemoglobin, water and melanin. Various approaches exist but in our initial work we have applied the simplest technique-the modified Beer–Lambert law. This method attempts to account for the spectral distortions introduced by multiple scattering via a simple linearised equation which relates overall tissue attenuation $-\ln(I/I_0)$ to the tissue absorption coefficient μ_a:

* Corresponding author. Tel.: +44-1234-754-767; fax: +44-1234-750-425
E-mail address: i.meglinski@cranfield.ac.uk (I.V. Meglinski).

$$A = -\ln\left(\frac{I}{I_0}\right) = \mu_a \sigma \rho + G \quad (1)$$

where ρ is the source–detector spacing and σ is a scaling factor, the 'differential pathlength factor' which accounts for the path lengthening effect of the random walk experienced by photons as they propagate through the multiple scattering medium. G is an offset term which is, according the Twersky's multiple-scattering theory [4,5], determined mainly by the tissue-probe geometry, or purely by the scattering.

Eq. (1) represents a linear relationship between $-\ln(I/I_0)$ and μ_a, then the technique of multilinear regression can be used to estimate the relative concentrations of chromophores in the skin, provided the wavelength dependence of G is known.

Since G is determined by scattering coefficient μ_s, then we will assume that it is dominated by a term of the form $a + b\lambda$. μ_a is given by the sum of absorption coefficients for each separate chromophore, which in turn are determined by the absolute concentration C and specific absorption coefficient ε of each chromophore. Given N chromophores, Eq. (1) can thus be rewritten:

$$A = a + b\lambda + \sum_{i=1}^{N} C_i \varepsilon_i(\lambda) \quad (2)$$

By making measurements of A at a minimum of $N+3$ wavelength, solving Eq. (2) for a, b and C_i's becomes an exercise in multi-linear regression which we solve using standard algorithms [6]. Typically we fit all wavelengths from 550 to 770 nm in 0.7 nm steps; hence the number of wavelength greatly exceeds N.

It should always be borne in mind however that Eq. (1) is simply an approximation. The modified Beer–Lambert law was originally introduced to analyze near-infrared transmission spectra of brain and muscles and, in particular, was designed to analyze relative changes in tissue oxygenation [7]. During such changes G and σ (see Eq. (1)) can, to first order, be assumed to remain unchanged so that Eq. (2), in the form:

$$\Delta A(\lambda) = \sum_{i=1}^{N} \Delta C_i \varepsilon_i(\lambda) \quad (3)$$

is used to estimate in oxy- and deoxy-hemoglobin concentration from changes in attenuation ΔA. The equation is strictly only valid in the limit that $\Delta C_i \to 0$, otherwise the fundamentally non-linear relationship between A and μ_a introduces errors. This effect has been studied using the diffusion equation for the specific case of detecting cytochrome–oxidase redox changes in the presence of large changes in hemoglobin absorption [8].

For this reason, it is one of the general goals of our Monte Carlo modeling to investigate the validity of the simple multi-linear regression approach. This can be done simply by comparing the actual chromophore concentrations used to perform Monte Carlo calculation with the chromophore concentrations extracted from the simulated reflectance spectrum by Eq. (2).

In this paper we present the method for the skin reflectance spectra simulation, that is done using the Monte Carlo technique. Different cells structure and blood distribution, variations of chromophores and water content in the skin layers affect their optical properties [9,10], which makes it difficult to define the optical events in a simulation. We simulate the absorption properties of skin layers corresponding to blood, water, melanin and overall chromophores content. Several efforts have been made to simulate the reflectance spectrum of skin relying on a diffusion approximation [11–14]. However, when the source–detector separation is 'small' (less than a few millimeters) diffusion approximation becomes invalid, and only the Monte Carlo technique can provide a realistic model of light propagation in biological tissues. The small source–detector separation is often preferred as it yields a shallow spatial location of the subject of study, which are capillary loops in our case. We propose more accurate model for correct prediction of the reflectance spectra measured by 'shallow' fiber-optic reflectance probe. In the paper we simply demonstrate the accuracy of the model by comparing the results of simulation and experimental results made in vivo.

2. Reflectance spectra simulation

2.1. Method

The skin reflectance spectra simulation is based on a Monte Carlo model developed recently [15,16]. In frame of the technique the simulation is performed as a sequential three dimensional tracing of photon packets between scattering events from the point of the radiation entering in medium, to the receiving area, where the photon leaves the medium. The random path that photons move at jth step is given by:

$$l_j = -\frac{\ln(\xi)}{\mu_s} \qquad (4)$$

where ξ is a uniformly distributed random number between 0 and 1. The scattering event is simulated by generating two random angles φ and θ in respect to the Henyey–Greenstein angular probability density function [17].

Internal reflection on the medium boundary is taken into account allowing the photon packet to split into a reflected and a transmitted part. The statistical weight of the reflected and transmitted parts of the photon packets is attenuated according to the Fresnel's reflection coefficients [18]:

The probability of the photon packet being detected can then be described as follows:

$$W = W_0 \prod_{k=1}^{M} R_k(\alpha_i) \qquad (6)$$

where W_0 is the initial weight of the photon packet in the medium, M is the number of photon packet partial reflections on the medium boundary.

The individual trajectory of each detected photon packet is stored in a data file, and then we include the absorption of the medium layers according the microscopic Beer–Lambert law:

$$I(\lambda) = \sum_{j}^{N_{ph}} W_j \exp\left(-\sum_{i=1}^{K_j} \mu_{ai}(\lambda)l_i\right) \qquad (7)$$

Here, W_j is the final weight of jth photon packet (see Eq. (6)), K_j is the total number of scattering events for the jth photon packet, μ_{ai} and l_i are the medium local absorption coefficient and pathlength of the photon packet at ith step, respectively. This approach is convenient for a rapid recalculation of the radiation intensity reflection for a various set of absorption coefficients $\mu_{ai}(\lambda)$, and their various derivatives for the unchanged source–detector configuration.

The total diffuse reflectance on the medium boundary is defined as the normalized sum of

$$R(\alpha_i) = \begin{cases} \left(\dfrac{n - n_0}{n + n_0}\right)^2, & \text{if} \quad \alpha_i = 0° \\[2mm] \dfrac{1}{2}\left[\dfrac{\sin^2(\alpha_i - \alpha_t)}{\sin^2(\alpha_i + \alpha_t)} + \dfrac{\tan^2(\alpha_i - \alpha_t)}{\tan^2(\alpha_i + \alpha_t)}\right], & \text{if} \quad 0° < \alpha_i < \sin^{-1}\left(\dfrac{n_0}{n}\right) \\[2mm] 1 & \text{if} \quad \sin^{-1}\left(\dfrac{n_0}{n}\right) < \alpha_i \leq 90° \end{cases} \qquad (5)$$

where α_i and α_t are the angles of the photon packet incidence on the medium boundary and angle of transmittance, respectively, n is the refractive index of the first layer of the medium and n_0 represents the refractive index of the ambient medium.

statistical weights of the photon packets reaching the detector area:

$$I/I_0 = \frac{1}{N_{ph}W_0} \sum_{j}^{N_{ph}} W_j \exp\left(-\sum_{i=1}^{K_j} \mu_{ai}(\lambda)l_i\right) \qquad (8)$$

Here, N_{ph} is the total number of detected photon packets (typically 10^5–10^6). The simulation of a photon packet is stopped if the photon statistical weight falls bellow 0.0001, or if a total number of scattering events exceed 10 000.

2.2. Skin model

Following earlier work aimed at the skin optical radiation dose modeling [9,14,19–21] we have considered skin as a three-dimensional half-infinite medium divided into seven layers. The first layer corresponds to the layer of desquamating flattened dead cells mainly containing keratin, which is 20 μm thick, and known as the stratum corneum. The second layer, we call Living epidermis, is 80–100 μm thick and is assumed to contain primarily living cells: a fraction of dehydrated cells, laden cells with keratohyalin granules, columnar cells, and also melanin dust, small melanin granules and melanosoms [1,2]. Given the inhomogeneous distribution of the blood vessels and skin capillaries within the skin [22] we sub-divide the dermis into four different layers, with different blood volumes. These layers are: pappilary dermis (150–200 μm thick), upper blood net dermis (80–100 μm thick), reticular dermis (1400–1600 μm thick), deep blood net dermis (80–120 μm thick). The deepest layer in our model is subcutaneous fat (6000–6500 μm thick).

2.3. Skin optics simulation

In the framework of our model we have calculated the absorption coefficients of dermal layers μ_a^{Layer} taking into account the spatial distribution of blood and water content within the skin, oxygen saturation S, and total hemoglobin volume fraction in blood γ:

$$\mu_a^{Layer}(\lambda) = (1-S)\gamma C_{Blood}\mu_a^{Hb}(\lambda) + S\gamma C_{Blood}\mu_a^{HbO_2}(\lambda)$$
$$+ (1-\gamma C_{Blood})C_{H_2O}\mu_a^{H_2O}(\lambda)$$
$$+ (1-\gamma C_{Blood})(1-C_{H_2O})\mu_a^{Other}(\lambda) \quad (9)$$

Here, $\mu_a^{HbO_2}(\lambda)$, $\mu_a^{Hb}(\lambda)$, $\mu_a^{H_2O}(\lambda)$ are the absorption coefficients of oxy- and deoxy-hemoglobin and water, respectively, C_{Blood} and C_{H_2O} are the layer
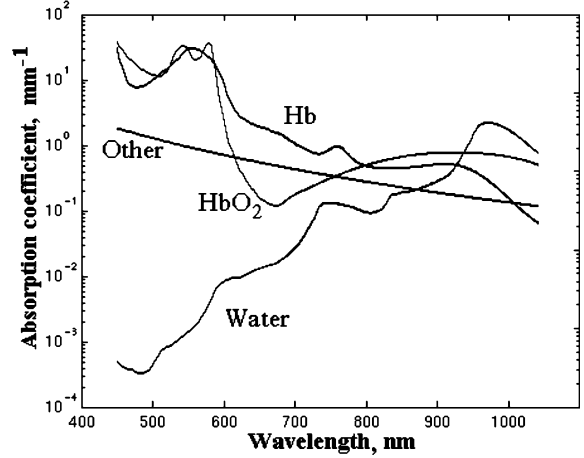

Fig. 1. The absorption coefficients of oxy- (HbO$_2$), deoxy- (Hb) hemoglobin, water (Water) and hemoglobin–water free tissues (Other) in visible and near infrared (NIR) range of spectra.

volume fractions of blood and water contents, and μ_a^{Other} is the absorption coefficient of the hemoglobin–water free tissue, defined as [23]:

$$\mu_a^{Other}(\lambda) = 7.84 \times 10^7 \times \lambda^{-3.255} \quad (10)$$

We have calculated γ assuming that hemoglobin is contained in the erythrocytes only, i.e.

$$\gamma = F_{Hb}F_{RBC}Ht \quad (11)$$

where Ht is the hemotocrit, F_{RBC} is the volume fraction of erythrocytes in the total volume of all blood cells, F_{Hb} is the volume fraction of hemoglobin in erythrocytes.

The absorption coefficients: $\mu_a^{Hb}(\lambda)$, $\mu_a^{HbO_2}(\lambda)$, $\mu_a^{H_2O}(\lambda)$ and $\mu_a^{Other}(\lambda)$ for the optical/NIR (400–1100 nm) range of spectrum are presented in Fig.

Table 1
Optical properties of the model of the human skin in the visible range of the spectrum ($\lambda = 633$ nm)

k	Name of layer	μ_s (mm^{-1})	g	n
1	Stratum corneum	100	0.86	1.5
2	Living epidermis	45	0.8	1.34
3	Papillary dermis	30	0.9	1.4
4	Upper blood net dermis	35	0.95	1.39
5	Reticular dermis	25	0.8	1.4
6	Deep blood net dermis	30	0.95	1.38
7	Subcutaneous fat	5	0.75	1.44

1. The absorption factors for oxy- and deoxy-hemoglobin and water are re-calculated from their spectra of extinction coefficients [24,25] with respect to their relative concentrations. In terms of optical density (1) measurements, absorption of water is significantly low relative to the absorption of oxy- and deoxy-hemoglobin. In a normal human skin, however, the content of water molecules is approximately 3×10^5 versus one molecule of hemoglobin [26]. Other skin layers optical properties used in the simulation: scattering coefficients μ_s, anisotropy factors g and refractive indices n are represented in Table 1. These data are collected from the literature: the scattering coefficients and anisotropy factors are taken from [9,10,27,28], and refractive indices from [9,29,30]. The values quoted at the wavelength $\lambda = 632$ nm. The refractive index of the ambient medium is taken to be $n_0 = 1$.

3. Results and discussions

The absorption coefficients calculated by Eq. (9) for the dermal layers are presented in Fig. 2. Parameters C_{Blood}, C_{H_2O}, S, Ht, F_{Hb}, F_{RBC} used for the calculation are presented in Table 2. These data are collected from a range of literature

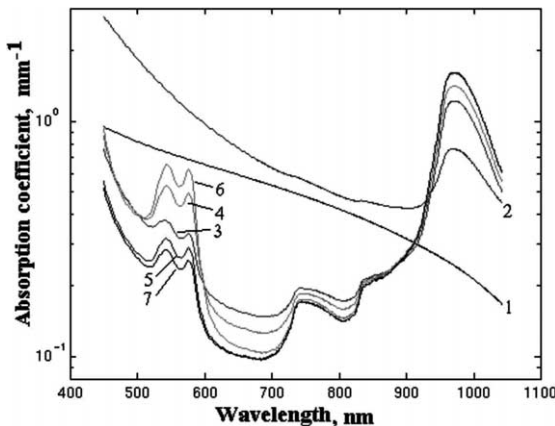
Fig. 2. Simulated absorption coefficients of skin layers: (1) stratum corneum; (2) living epidermis; (3) pappilary dermis; (4) upper blood net dermis; (5) reticular dermis; (6) deep blood net dermis; (7) subcutaneous fat.

[1,2,22,26,31–35], that, we believe, is corresponded to skin at normal stage.

Absorption coefficients for the blood free layers of skin, i.e. for stratum corneum and living epidermis, are calculated similar to what is proposed in [10]. We assume that $\mu_a(\lambda)$ of stratum corneum is described as:

$$\mu_a^{Stratum}(\lambda) = (0.1 - 8.3 \times 10^{-4} \times \lambda) + 0.125 \times \mu_a^{Other}(\lambda) \quad (12)$$

and for living epidermis water content and the experimental data [36,37] are taken into account:

$$\mu_a^{living_{epidermis}}(\lambda) = (0.5 \times 10^{10} \times \lambda^{-3.33})(1 - C_{H_2O}) + C_{H_2O}\mu_a^{H_2O}(\lambda) \quad (13)$$

The results of the simulation (see Fig. 2) are well agreed with the experimental results for Caucasian skin [38], and have showed that absorption of the visible/NIR radiation in stratum corneum and living epidermis decreases uniformly with wavelength from 450 to 900 nm. The peaks at 970–980 nm featured in all layers, except stratum corneum, are produced by the water absorption (see Fig. 1 and Table 2).

As one can see from Fig. 2 in the blood containing layers (i.e. pappilary dermis, upper blood net dermis, reticular dermis, deep blood net dermis and subcutaneous fat) the absorption of oxy- and deoxy-hemoglobin dominates for the wavelength shorter than 600 nm (see Fig. 1 for comparison). In the range of 600–800 nm the absorption is minimum (see Fig. 2).

Using the optical properties we simulate the skin reflectance spectra by the Monte Carlo technique described above. We have found that the results of simulation are remarkably similar to the experimental results of skin spectra measurements in visible (450–600 nm) range of spectrum (Fig. 3).

The measured reflectance spectra of skin are obtained by the spectrophotometer system described in detail earlier [39,40]. In short, the skin reflectance spectra are collected from the surface of the tissue with a pair of optical fibers separated at fixed distance (400 μm). The detected fiber collects light within a range of angles defined by

Table 2
The parameters used in the calculation of the absorption coefficients of the blood contented layers of the skin

k	Name of layer	C_{Blood}	S	Ht	F_{Hb}	F_{RBC}	C_{H_2O}
1	Stratum corneum	0	0	0	0	0	0.05
2	Living epidermis	0	0	0	0	0	0.2
3	Papillary dermis	0.04	0.6	0.45	0.99	0.25	0.5
4	Upper blood net dermis	0.3	0.6	0.45	0.99	0.25	0.6
5	Reticular dermis	0.04	0.6	0.45	0.99	0.25	0.7
6	Deep blood net dermis	0.1	0.6	0.45	0.99	0.25	0.7
7	Subcutaneous fat	0.05	0.6	0.45	0.99	0.25	0.7

C_{Blood} derived from Refs. [1,2,22,26,31–34] and personnel communication with Professor A. Shore, C_{H_2O} evaluated from Refs. [26,35], S, Ht, F_{Hb}, F_{RBC} derived from Refs. [22,26,32] and personnel communication with Professor A. Shore.
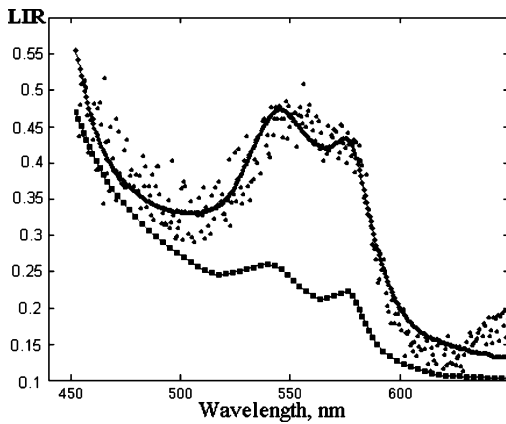

Fig. 3. The skin reflectance spectra: rhombuses and dots represent the results of simulated and measured reflectance spectra, respectively. Squares are the results of skin spectrum simulation with the 40% reduction of blood volume in the first two dermal layers (i.e. in pappilary dermis and upper blood net dermis). LIR is defined as the logarithm to the base 10 of the inverse reflectance ($R = I/I_0$), i.e. $\log_{10}(1/R)$ or $\log_{10}(1/W)$, respectively.

the numerical aperture. A quartz halogen lamp is used as an optical/NIR source of light, and a spectrograph/monochromator with a CCD camera is used for high speed spectra measurements, where one dimension is responsible for wavelength and the other for the intensity of detected scattering light. Our choice of source–detector optical fibers spacing is based on the results of spatial sensitivity study reported recently [15,16]. In these studies we showed that for 400 μm source–detector spacing the main part of detected signal becomes localized in the topical skin layers includ-

ing pappilary dermis and upper blood net dermis. The results of reflectance spectra simulation in case of 40% blood content reduction in topical dermal layers (i.e. pappilary dermis and upper blood net dermis) (see Fig. 3) well illustrate what happens if the absorption properties of the skin are changed. An increase of the blood content in the upper layers will tend to reduce the overall path length in that layers, conversely a decrease in blood content will lengthen the path length in it. However, we believe that amount of blood used in our simulation (see Table 2) was reliably estimated for the true blood content in the skin tissues at normal stage. These results are agreed with the results of independent study of the skin color variations [41].

We have presented the visible spectral region only, as it was best fitted (see Fig. 3). The difference in the results of simulation and experimental data (see Fig. 3) could be explained by our choice of the optical properties of the skin tissues for the simulation, and possible experimental errors. In the model we did not include the influence of various pigments as melanin, bilirubin, NADH, β-carotine and other chromophores [3], temperature dependence and some physiological parameters. In frame of the proposed model shape of the simulated skin spectra is determined by the combination of spectra of oxy- and deoxyhemoglobin, water and summarized absorption of other chromophores. We simulated the skin reflection spectra assuming the wavelength independence of the skin layers scattering (μ_s and g are constant, see Table 1). Whereas, in reality the

scattering of skin tissues tends to monotonously decrease from 450 to 1100 nm [28,29], and the difference in scattering at 450–600 and 700–1100 nm ranges is significant. Nevertheless, the results of simulation show that in the range of spectra where the scattering of skin tissues is changed slightly, it is possible to compare the experimental and modeling results quantitatively.

4. Summary

The reflectance spectra of human skin have been studied to support the theoretical model of skin tissues optical properties. The reflectance spectra of human skin simulated by the Monte Carlo technique and measured in vivo are in good agreement with one another. The modeling results are a brief survey of the potential of the computer simulation of skin reflectance spectra. Presented approach can be considered for use in studies of oxygen saturation of blood, skin chromophores, pigmentation, erythema and skin color changing. The model fitting based on the multi-linear regression analysis can give us quantitative amount of skin chromophores of the interest. Including in the model the wavelength dependence of G (see Eq. (1)) it is possible to extend the boundaries of the spectral region for the quantitative model fitting in NIR spectral area in the future.

References

[1] K.S. Stenn, The skin, in: L. Weiss (Ed.), Cell and Tissue Biology, Urban & Shwarzenberg, Baltimore, MD, 1988, pp. 541–572.

[2] G.F. Odland, Structure of the skin, in: L.A. Goldsmith (Ed.), Physiology, Biochemestry and Molecular Biology of the Skin, vol. I, Oxford University Press, Oxford, 1991, pp. 3–62.

[3] A.R. Young, Chromophores in human skin, Phys. Med. Biol. 42 (1997) 789–802.

[4] V. Twersky, Multiple scattering of waves and optical phenomena, JOSA 52 (1962) 145–171.

[5] V. Twersky, Absorption and multiple scattering by biological suspensions, JOSA 60 (1970) 1084–1093.

[6] W.H. Press, S.A. Teukolsky, W.T. Vetterling, B.P. Flannery, Numerical Recipes in C, 2nd ed., Cambridge University Press, Cambridge, 1992.

[7] D.T. Delpy, M. Cope, P. van der Zee, S.R. Arridge, S. Wray, J. Wyatt, Estimation of optical pathlength through tissue from direct time of flight measurement, Phys. Med. Biol. 33 (1988) 1433–1442.

[8] S.J. Matcher, C.E. Elwell, C.E. Cooper, M. Cope, D.T. Delpy, Performance comparison of several published tissue near-infrared spectroscopy algorithms, Anal. Biochem. 227 (1995) 54–68.

[9] V.V. Tuchin, Tissue Optics: Light Scattering Methods and Instruments for Medical Diagnosis, SPIE—The International Society for Optical Engineering, Washington, DC, 2000.

[10] S.L. Jacques, Origins of tissue optical properties in the UVA, visible and NIR regions, in: R.R. Alfano, J.G. Fujimoto (Eds.), Advances in Optical Imaging and Photon Migration, vol. 2, Optical Society of America (OSA), Washington, DC, 1996, pp. 364–370.

[11] S. Wan, R.R. Anderson, J.H. Parrish, Analytical modeling for the optical properties of the skin with in vitro and in vivo applications, Photochem. Photobiol. 34 (1981) 493–499.

[12] P.H. Andersen, P. Bjerring, Noninvasive computerized analyses of skin chromophores in vivo by reflectance spectroscopy, Photodermatol. Photoimmunol. Photomed. 7 (1990) 249–257.

[13] L.T. Norvang, E.J. Fiskerstrand, K. Koenig, B. Bakken, D. Grini, O. Standahl, T.E. Milner, M.W. Berns, J.S. Nelson, L.O. Svaasand, Comparison between reflectance spectra obtained with an integrating sphere and a fiberoptic collection system, in: G.P. Delacretaz, R.W. Steiner, L.O. Svaasand, H.J. Albrecht, T.H. Meier (Eds.), Laser–Tissue Interaction and Tissue Optics, Proc. SPIE, vol. 2624, 1995, pp. 155–164.

[14] G. Kumar, J.M. Schmitt, Optimum wavelength for measurement of blood hemoglobin content tissue hydration by NIR spectroscopy, in: D.L. Farkas, R.C. Leif, A.V. Priezzhev, T. Asakura, B.J. Tromberg (Eds.), Optical Diagnostics of Living Cells and Biofluids, Proc. SPIE, vol. 2678, 1996, pp. 442–453.

[15] I.V. Meglinskii, S.J. Matcher, The analysis of spatial distribution of the detector depth sensitivity in multi-layered inhomogeneous highly scattering and absorbing medium by the Monte Carlo technique, Opt. Spectrosc. 91 (2001) 654–659.

[16] I.V. Meglinsky, S.J. Matcher, Modeling the sampling volume for the skin blood oxygenation measurements, Med. Biol. Eng. Comput. 39 (2001) 44–50.

[17] L.G. Henyey, J.L. Greenstein, Diffuse radiation in the galaxy, Astrophys. J. 93 (1941) 70–83.

[18] M. Born, E. Wolf, Principles of Optics: Electromagnetic Theory of Propagation, Interference and Diffraction of Light, 6th ed., Pergamon Press, New York, 1986.

[19] M. Keijzer, S.L. Jaques, S.A. Prahl, A.J. Welch, Light distribution in artery tissue: Monte Carlo simulation for finite-diameter laser beams, Lasers Surg. Med. 9 (1989) 148–154.

[20] I.V. Yaroslavsky, V.V. Tuchin, Light propagation in multilayer scattering media: modeling by the Monte Carlo method, Opt. Spectrosc. 72 (1992) 505–509.

[21] S.L. Jaques, L. Wang, L.-Q. Zheng, MCML-Monte Carlo modeling of photon transport in multi-layered tissues, Comput. Methods Programs Biomed. 47 (1995) 131–146.

[22] T.J. Ryan, Cutaneous circulation, in: L.A. Goldsmith (Ed.), Physiology, Biochemistry and Molecular Biology of the Skin, vol. II, Oxford University Press, Oxford, 1991, pp. 1019–1084.

[23] I.S. Saidi, Transcutaneous optical measurement of hyper-bilirubinemia in neonates, PhD thesis, Rice University, Houston, TX, 1992.

[24] W.G. Zijlstra, A. Buursma, W.P. Meeuwsen-van der Roest, Absorption spectra of human fetal and adult oxyhemoglobin, de-oxyhemoglobin, carboxyhemoglobin, and methemoglobin, Clin. Chem. 37 (1991) 1633–1638.

[25] G.M. Hale, M.R. Querry, Optical costants of water in the 200-nm to 200-μm wavelength region, Appl. Opt. 12 (1973) 555–653.

[26] G. Chapman, The Body Fluids and Their Functions, Edward Arnold, London, 1980.

[27] C.R. Simpson, M. Kohl, M. Essenpreis, M. Cope, Near-infrared optical properties of ex vivo human skin and subcutaneous tissues measured using the Monte Carlo inversion technique, Phys. Med. Biol. 43 (1998) 2465–2478.

[28] R.M.P. Doornbos, R. Lang, M.C. Aalders, F.M. Cross, H.J.C.M. Sterenborg, The determination of in vivo human tissue optical properties and absolute chromophore concentrations using spatially resolved steady-state diffuse reflectance spectroscopy, Phys. Med. Biol. 44 (1999) 967–981.

[29] S. Gonzalez, M. Rajadhyaksha, R.R. Anderson, Non-invasive (real-time) imaging of histologic margin of a proliferative skin lesion in vivo, Int. Invest. Dermat. 111 (1998) 538–539.

[30] G.J. Tearney, M.E. Brezinski, J.F. Southern, B.E. Bouma, M.R. Hee, J.G. Fujimoto, Determination of the refractive index of highly scattering human tissue by optical coherence tomography, Opt. Lett. 20 (1995) 2258–2260.

[31] R. Bull, G. Ansell, A.W.B. Stanton, J.R. Levick, P.S. Mortimer, Normal cutaneous microcirculation in gaiter zone (ulcer-susceptible skin) versus nearby regions in healthy young adults, Int. J. Microcirc. 15 (1995) 65–74.

[32] D. MacN. Surgenor (Ed.), The Red Blood Cells, Academic Press, New York, 1975.

[33] A. Ikeda, N. Umeda, K. Tsuda, S. Ohta, Scanning electron microscopy of the capillary loops in the dermal papillae of the hand in primates, including man, J. Electron Microsc. Tech. 19 (1991) 419–28.

[34] A.J. Jaap, A.C. Shore, A.J. Stockman, J.E. Tooke, Skin capillary density in subject with impaired glucose tolerance and patients with type 2 diabetes, Diabet. Med. 13 (1996) 160–164.

[35] R.O. Potts, Stratum corneum hydration: experimental techniques and interpretations of results, J. Soc. Cosmet. Chem. 37 (1985) 9–33.

[36] R.R. Anderson, J. Hu, J.A. Parrish, Optical radiation transfer in the human skin and applications in in vivo remittance spectroscopy, in: R. Marks, P.A. Payne (Eds.), Bioengineering and the Skin, MTP Press, Boston, MA, 1979, pp. 253–265.

[37] J.W. Feather, J.B. Dawson, D.J. Barker, J.A. Cotterill, A theoretical and experimental study of the optical properties of in vivo skin, in: R. Marks, P.A. Payne (Eds.), Bioengineering and the Skin, MTP Press, Boston, MA, 1979, pp. 275–281.

[38] R. Marchesini, C. Clemente, E. Pignoli, M. Brambilla, Optical properties of in vivo epidermis and their possible relationship with optical properties of in vivo skin, J. Photochem. Photobiol. B: Biol. 16 (1992) 127–140.

[39] M. Cope, D.T. Delpy, J.S. Wyatt, S.C. Wray, E.O.R. Reynolds, A CCD spectrometer to quantitate the concentration of chromophores in living tissue utilising the water absorption peak of water at 975 nm, Adv. Exp. Med. Biol. 247 (1989) 33–41.

[40] M. Osawa, S. Niwa, A portable diffuse reflectance spectrophotometer for rapid and automatic measurement of tissue, Meas. Sci. Technol. 4 (1993) 668–676.

[41] W. Verkruysse, G.W. Lucassen, M.J.C. van Gemert, Simulation of color of port wine stain skin and its dependence on skin variables, Lasers Surg. Med. 25 (1999) 131–139.